

Journal Pre-proof

Electrical and magnetic properties of $\text{La}_{1-x}\text{Ag}_x\text{MnO}_3$ ($0 \leq x \leq 0.5$) polycrystalline ceramics by combination of first principles calculations and experimental methods

Shuai Zhang, Tao Sun, Fuquan Ji, Gang Dong, Yang Liu, Zhidong Li, Hui Zhang, Qingming Chen, Xiang Liu

PII: S0925-8388(19)32942-1

DOI: <https://doi.org/10.1016/j.jallcom.2019.151709>

Reference: JALCOM 151709

To appear in: *Journal of Alloys and Compounds*

Received Date: 24 April 2019

Revised Date: 31 July 2019

Accepted Date: 4 August 2019

Please cite this article as: S. Zhang, T. Sun, F. Ji, G. Dong, Y. Liu, Z. Li, H. Zhang, Q. Chen, X. Liu, Electrical and magnetic properties of $\text{La}_{1-x}\text{Ag}_x\text{MnO}_3$ ($0 \leq x \leq 0.5$) polycrystalline ceramics by combination of first principles calculations and experimental methods, *Journal of Alloys and Compounds* (2019), doi: <https://doi.org/10.1016/j.jallcom.2019.151709>.

This is a PDF file of an article that has undergone enhancements after acceptance, such as the addition of a cover page and metadata, and formatting for readability, but it is not yet the definitive version of record. This version will undergo additional copyediting, typesetting and review before it is published in its final form, but we are providing this version to give early visibility of the article. Please note that, during the production process, errors may be discovered which could affect the content, and all legal disclaimers that apply to the journal pertain.

© 2019 Published by Elsevier B.V.



Electrical and magnetic properties of $\text{La}_{1-x}\text{Ag}_x\text{MnO}_3$ ($0 \leq x \leq 0.5$) polycrystalline ceramics by combination of first principles calculations and experimental methods

Shuai Zhang, Tao Sun, Fuquan Ji, Gang Dong, Yang Liu, Zhidong Li, Hui Zhang,

Qingming Chen, Xiang Liu*

(School of Material Science and Engineering, Kunming University of Science and Technology, Kunming 650093, Yunnan, China)

Abstract

In this work, electrical and magnetic properties of $\text{La}_{1-x}\text{Ag}_x\text{MnO}_3$ (LAMO, $0 \leq x \leq 0.5$) polycrystalline ceramics with double-exchange (DE) effect and Jahn-Teller (JT) distortion were studied using a combination of first principles calculations and experimental methods. The GGA + U method was used to correct the self-interaction error (SIE) that was encountered in first principles calculations. With the increasing of Ag, energy band gaps (E_i or E_d) of LAMO ceramics and the JT effect decreased, while the DE effect was enhanced. LAMO polycrystalline ceramics ($x = 0, 0.1, 0.2, 0.3, 0.4$ and 0.5) were prepared by conventional sol-gel method in order to verify the calculation results. The X-ray diffraction revealed that the structure of LAMO ceramics transformed from single phase to multiphase as x was increased. The ρ - T

* Corresponding author

E-mail address: lxjim@sina.com

curves suggested that the metal to insulator transition temperature (T_p) and DE effect were improved as x increased, which was in good agreement with the first principles calculations. In addition, the temperature coefficient of resistance (TCR) at the peak temperature (T_k) and magnetoresistance (MR) at the peak temperature (T_m) were obtained with different x . For $x = 0.5$, the value of TCR and MR reached $8.58\% \text{ K}^{-1}$ and 21.6% , and the T_p , T_k and T_m were 304, 291 and 298 K, respectively, implying that the electrical and magnetic devices of LAMO ceramics could operate at room temperature (300 K). XPS results indicated that the concentration of Mn^{4+} ion increased with increasing x . The ratio of $\text{Mn}^{4+}/\text{Mn}^{3+}$ reached 1 : 2, which had the strongest DE and magnetoelectric coupling effect for $x = 0.5$.

Keywords: Electronic structure; Double-exchange (DE) effect; Temperature coefficient of resistance (TCR); Magnetoresistance (MR)

1. Introduction

Doped manganite based on $\text{R}_{1-x}\text{A}_x\text{MnO}_3$ (R = rare-earth ion, such as La, Pr, Nd and A = divalent elements, such as Ca, Sr, Ba) polycrystalline ceramics have been intensively studied [1-6] due to their interesting physical properties such as colossal magnetoresistance (CMR) [7], metal-insulator (M-I) transition at room temperature, thermoelectric properties [8-10], data storage and magneto refractive effect [11-13]. The double-exchange (DE) mechanism [14, 15] based on the Hund coupling of the e_g and t_{2g} electrons played a key role in the understanding of perovskite magnetic and electrical properties, and hopping of e_g electrons between Mn^{3+} and Mn^{4+} ions. However, Millis *et al.* [15] argued that the CMR in $\text{R}_{1-x}\text{A}_x\text{MnO}_3$ polycrystalline

ceramics could not be interpreted by DE alone, and various other factors such as Jahn–Teller (JT) effect need to be considered. The JT effect changed the Mn–O bond lengths and also introduced distortion in the MnO_6 octahedron.

Recent studies have focused on divalent doping in LaMnO_3 (LMO) polycrystalline ceramics [2, 16, 17]. However, compared with divalent doped manganites, monovalent metal doping (such as Ag, Na, K) still need further investigation ascribing to its significant electrical and magnetic properties. In addition, the monovalent doping in LMO has similar *CMR* and M–I transition properties compared to divalent doping, but different charge, spin and lattice interactions due to differences in valence and ion size. The temperatures of M–I transition (T_p) have also been studied from 180~340 K for $\text{La}_{1-x}\text{A}_x\text{MnO}_3$ (A = Na, K, Ag) in previous studies [4, 12, 13, 18]. However, among these polycrystalline ceramics in $\text{La}_{1-x}\text{A}_x\text{MnO}_3$, there haven't been detailed studies focusing on room temperature T_p or the combination of DE and JT effects. Thus, in this paper, the effect of Ag doping LMO on structural and electronic transport properties were studied using a combination of experimental methods and first principles calculations. High *TCR* and *MR* near room temperature were obtained for $\text{La}_{1-x}\text{Ag}_x\text{MnO}_3$ (LAMO) polycrystalline ceramics. The Cambridge sequential total energy package (CASTEP) code, and general gradient approximation (GGA) with Perdew–Burke–Ernzerhof (PBE) from first principles were carried out [19]. In order to correct for the self-interaction error (SIE), the GGA + U approach [20-24] was adopted to improve the accuracy of calculations, with $U = 2.5$ eV being applied in the Mn *3d* state. The total and partial electronic densities of states (DOS, PDOS)

suggested that the DE and J–T effect intensified and diminished with increasing x , respectively, which was in consistent with the experimental ρ – T curves.

2. Method and details

2.1. Computation details

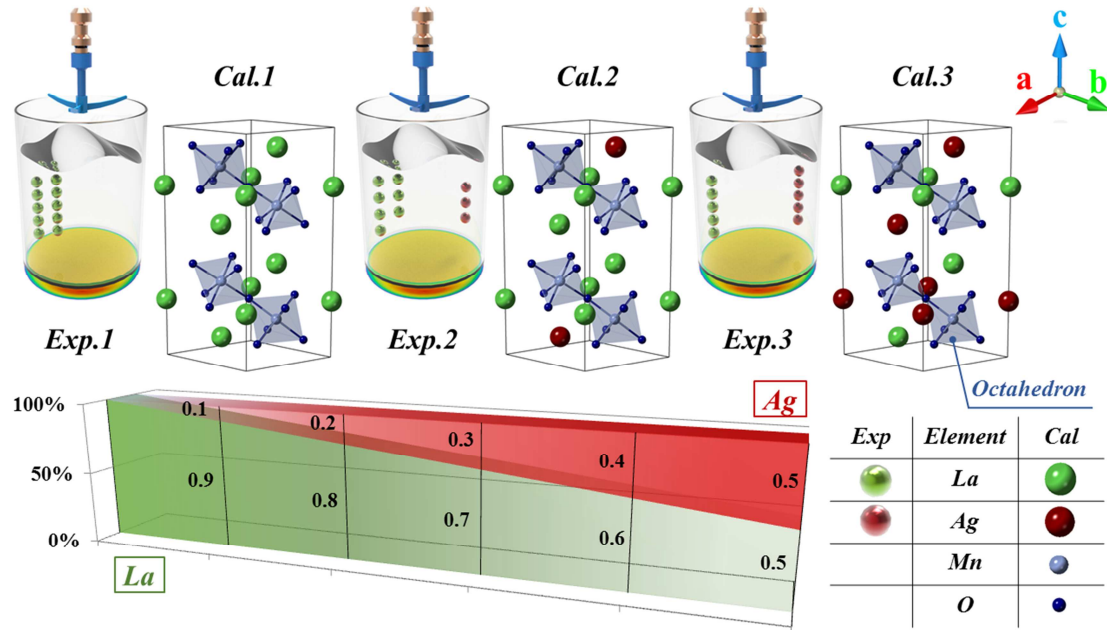


Fig.1. Schematic of unit cell structure of LAMO ($x = 0, 0.3, 0.5$) for first principles calculations.

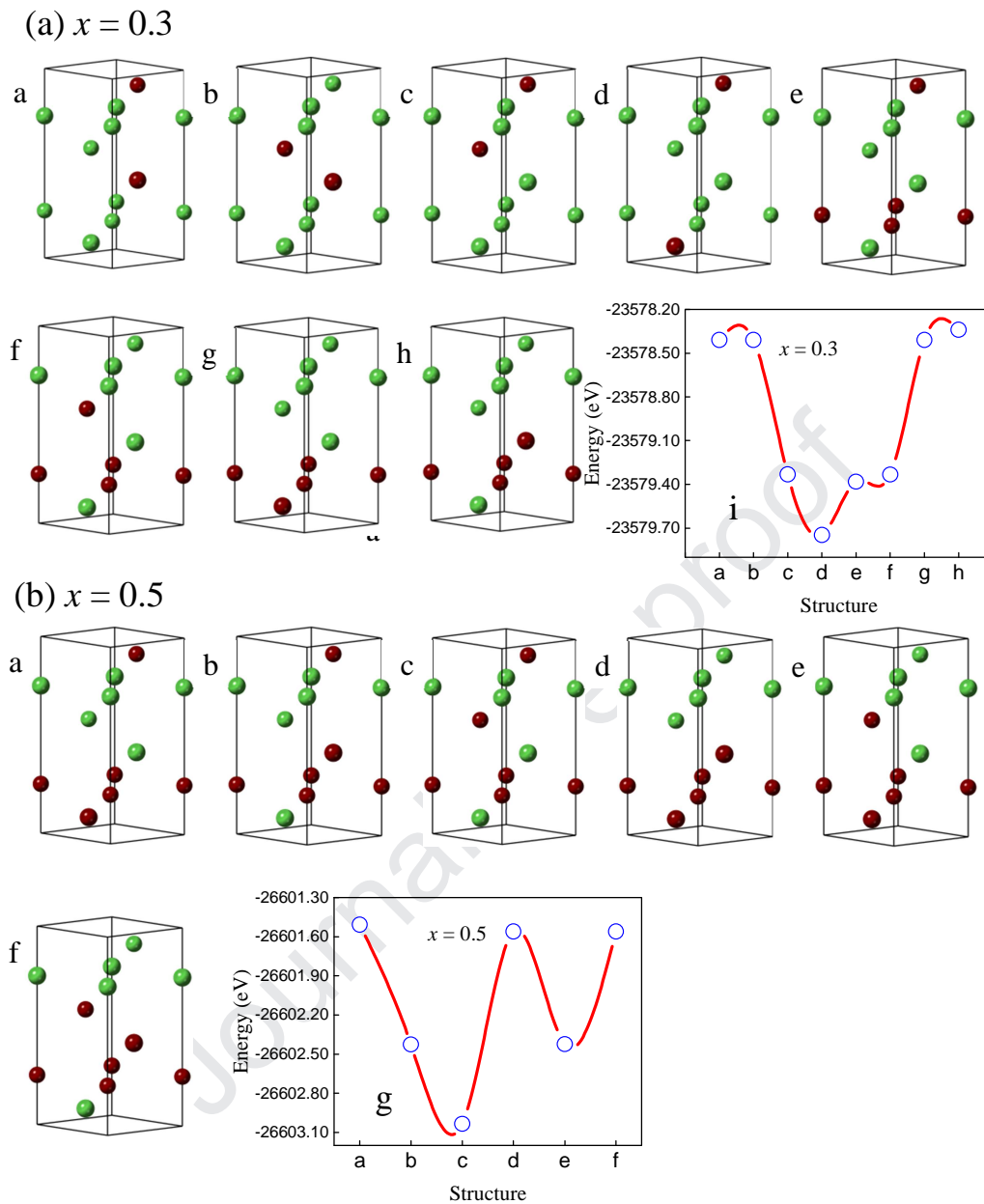


Fig.2. La/Ag relative configurations structures and energy as a function of structure for LAMO ($x = 0.3, 0.5$) ceramics, respectively. (a): $x = 0.3$, different Ag atom location structure (a ~ h) and energy versus structure curves (i) for LAMO ceramics. (b): $x = 0.5$, different Ag atom location structure (a ~ f) and energy versus structure curves (g) for LAMO ceramics. Here, La and Ag atoms represent in green and dark red colors, respectively.

As shown in Fig 1, the sol-gel method was used for experiments and calculations were performed based on density functional theory (DFT) for LAMO crystal rhombohedral structure with space group $R\bar{3}c$. The electronic structure of LAMO

was investigated theoretically by first principles using the GGA + U approach. In order to obtain the most stable structure from first principles calculations, different La/Ag ratios were considered for LAMO ($x = 0.3, 0.5$) ceramics, as shown in Fig 2. The energy as a function of structure was also studied, as shown in Fig 2 (a) i and (b) g. Since the structures of d for $x = 0.3$ and c for $x = 0.5$ had the lowest energy, and they were chosen for the calculations for this work. The different proportions of La atoms in the A site were substituted by Ag for LAMO perovskite structure [17, 20]. All calculations were carried out by the CASTEP code, and utilizing the GGA (PBE) with Coulomb correlations ($U = 2.5$ eV). We employed a $1 \times 1 \times 1$ unit cell LAMO rhombohedral perovskite with lattice parameters $a = b = 5.518$ Å and $c = 13.355$ Å, which contained 12 La atoms, 16 Mn atoms and 18 O atoms, as shown in Fig 1. The cut-off energy of 500 eV and a $5 \times 4 \times 5$ Monkhorst-pack k-point mesh in the Brillouin zone were employed to obtain the reliable calculation results. In addition, the electronic and ionic convergence tolerance for geometry optimization was set to 5×10^{-6} eV and 0.01 eV/Å, respectively. The maximum stress within 0.02 GPa, and the max displacement using 5×10^{-4} Å.

2.2. Experimental method

Bulk polycrystalline LAMO ($x = 0, 0.1, 0.2, 0.3, 0.4$ and 0.5) ceramics were prepared by the sol-gel method. The starting materials composed of $\text{La}(\text{NO}_3)_3 \cdot n\text{H}_2\text{O}$ (99.99%, from sinopharm chemical reagent), $\text{Mn}(\text{NO}_3)_2$ aqueous solutions (50% by mass, from sinopharm chemical reagent) and AgNO_3 (from sinopharm chemical reagent), were dissolved in 200 ml deionized water under continuous stirring. Citric

acid and ethylene were used as complexing and polymerizing agents, respectively. The mixture was heated until a foamed gel was formed by magnetic stirrers. Then, the foamed gel was dried at 140 °C for 12 h and ground into powders. The powders were then pre-sintered at 900 °C for 12 h and pressed into pellets at a pressure of 16 MPa. Finally, pellets were synthesized at 1100 °C for 12 h.

The structure of the prepared LAMO ceramics was characterized by X-ray diffraction (XRD, Rigaku Ultima IV) measurements with Cu K α radiation. The grain sizes and morphology were examined by field emission scanning electron microscopy (FESEM, HITACHI, SU8010). The electromagnetic performance indicators were measured by conventional four-probe method at temperature ranging from 100 to 320 K and external field of 1 T using Keithley Instruments. X-ray photoemission spectroscopy (XPS) was employed to study the stoichiometry and valence state of polycrystalline ceramics.

3. Results and discussion

3.1. Calculation of electronic structure

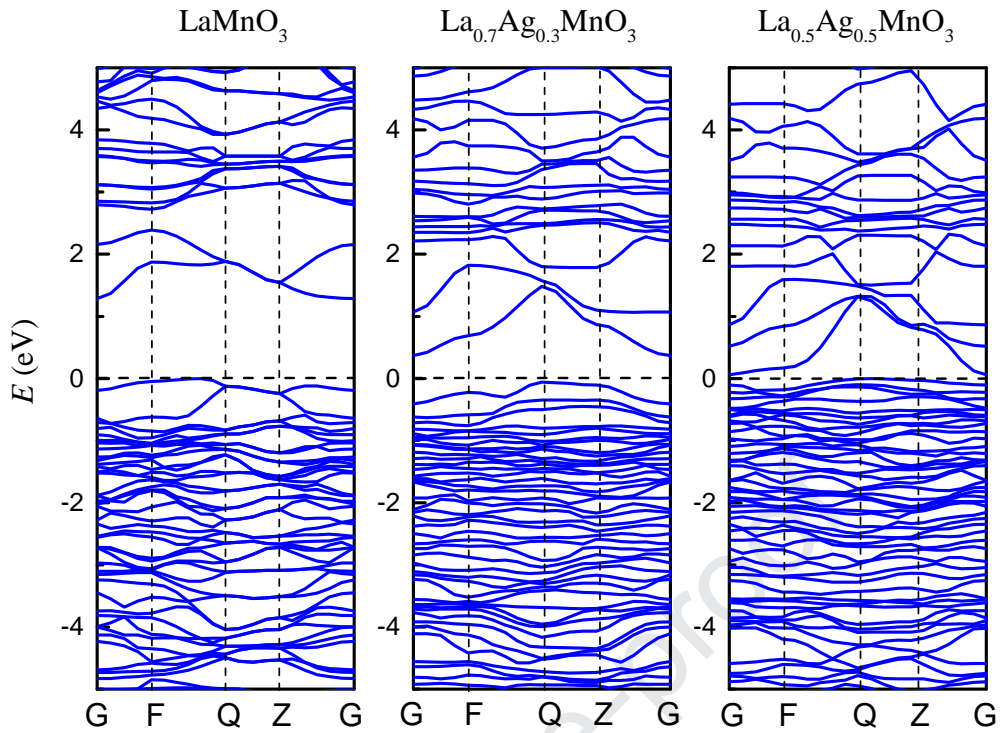


Fig.3. Band structure for $\text{La}_{1-x}\text{Ag}_x\text{MnO}_3$ ($x = 0, 0.3, 0.5$)

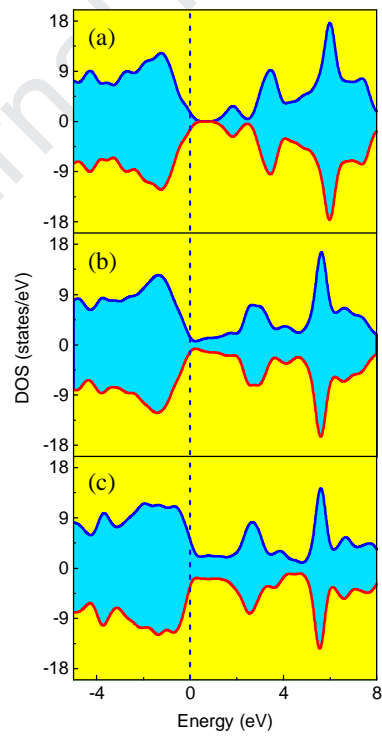


Fig.4. Density of states (DOS) of different Ag doping level for LAMO: (a) LaMnO₃, (b) La_{0.7}Ag_{0.3}MnO₃ and (c) La_{0.5}Ag_{0.5}MnO₃.

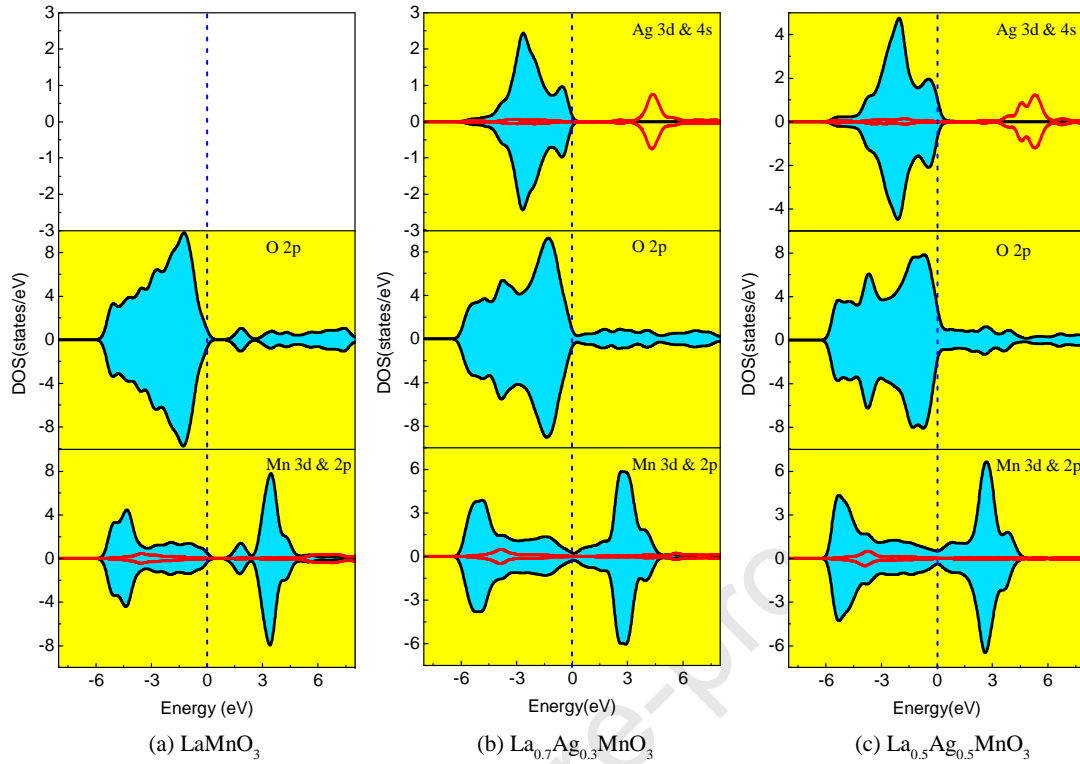


Fig.5. Partial DOS (PDOS) of LAMO ($x = 0, 0.3, 0.5$): (a) LaMnO_3 , (b) $\text{La}_{0.7}\text{Ag}_{0.3}\text{MnO}_3$, and (c) $\text{La}_{0.5}\text{Ag}_{0.5}\text{MnO}_3$. For Ag and Mn orbital DOS, the black and the red curves represents the 4d, 4s and 3d, 2p orbitals, respectively.

Table.1.

Indirect (E_i) and direct energy band gap (E_d), Mn magnetic moment and average atomic partial charge (q) from band analysis for LAMO ($x = 0, 0.3, 0.5$) polycrystalline ceramics.

x (mol%)	0	0.3	0.5
E_i (eV)	1.29	0.37	0.06
E_d (eV)	1.51	0.79	0.23
μ_{Mn} (μ_{B})	4.06	3.63	3.33
q_{Mn} (e)	0.62	0.68	0.74
q_{Ag} (e)	0.0	0.22	0.38

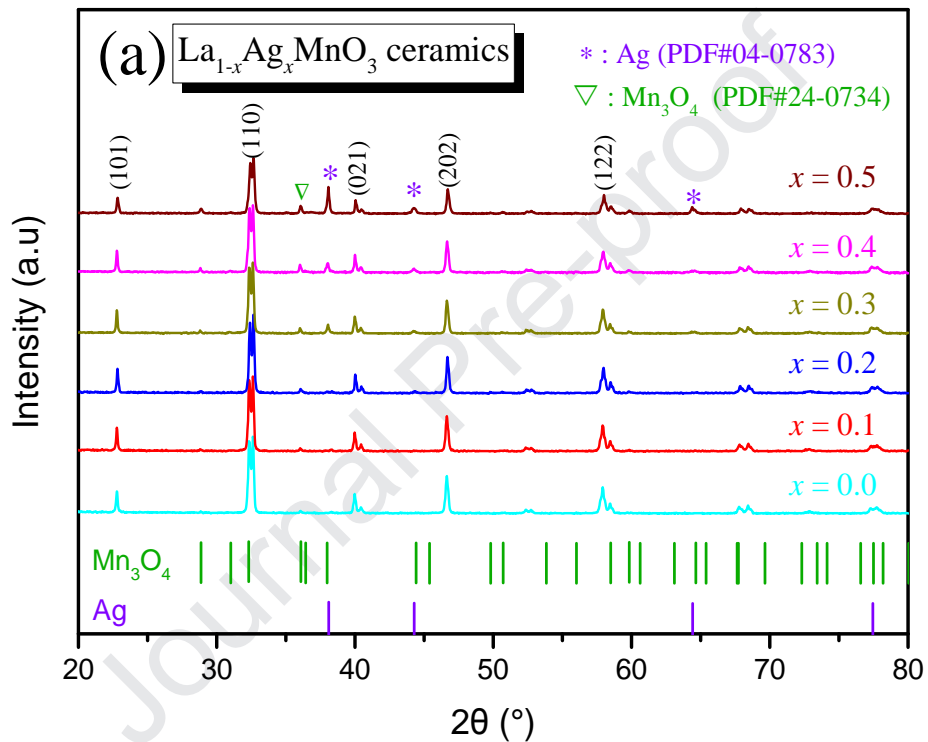
The band structure, Mn magnetic moment and average atomic partial charge (q) obtained from first principles for LAMO ($x = 0, 0.3$ and 0.5) are shown in Fig 3 and Table 1. From the band structure it is evident that all the structures exhibited insulating characteristics. The direct band gap (E_d) was ~ 1.51 , ~ 0.79 and ~ 0.23 eV

for $x = 0, 0.3$ and 0.5 , respectively. This decrease of band gap with increasing x can be attributed to the change of spin polarization that resulting in a faint splitting of Mn 3d. Meanwhile, E_d of 1.51 eV for LMO was in good agreement with previous experimental reports, which were in the range of 1.1~2.0 eV [25, 26], and also similar to the previous calculation studies which reported values of 1.427 eV [24], 1.21 eV [27] and 1.64 eV [23]. In addition, as x increased, the Mn magnetic moment (μ_B) decreased from 4.06 to 3.33 μ_B . The average atomic partial charge (q_{Mn}) increased from 0.62 to 0.74 e with Ag contents increasing, indicated that Ag doping results the concentration of Mn³⁺ decreased and Mn⁴⁺ enhanced.

The DOS and PDOS (Ag, O, Mn) for the different of x are shown in Fig 4 and Fig 5. By combining with Fig 3, it was clear that the Mn e_g ($e_{g\uparrow}^1$ and $e_{g\uparrow}^2$) splitting reduced with increasing x , and hybridization between Ag 4d and O 2p orbitals enhanced. The Mn $e_{g\uparrow}^1$ and $e_{g\uparrow}^2$ orbitals located at the top of valence and the bottom of conduction band, and O 2p orbitals above Mn t_{2g}^3 states dominated the valence band. Mn t_{2g}^3 orbitals shifted to low energy in valence and conduction band. In addition, the energy separation of $E(e_{g\uparrow}^2) - E(e_{g\uparrow}^1)$ resulted from the JT splitting band based on previous work [28]. $E(e_{g\uparrow}^2) - E(e_{g\uparrow}^1)$ corresponded to the indirect band gap (E_i) and decreased from 1.29 to 0.06 eV, which suggested that the JT effect diminished with increasing x . The DE effect based on the Hund coupling between Mn e_g and t_{2g}^3 electron was also studied as a function of x , as shown in Fig. 5. Due to the strong orbital overlap of Mn e_g and O 2p, the energy difference between Mn t_{2g}^3 and O 2p orbital was regarded as the energy difference between Mn t_{2g}^3 and e_g . As a

result, Mn t_{2g}^3 and O 2p were respectively shifted to low energy and high energy in valence band as x increased. This indicated that the energy difference between Mn t_{2g}^3 and O 2p orbital was augmented. Therefore, the energy difference of the Hund coupling between e_g and t_{2g}^3 increased, and indicated DE effect was enhanced.

3.2. Analysis of structural



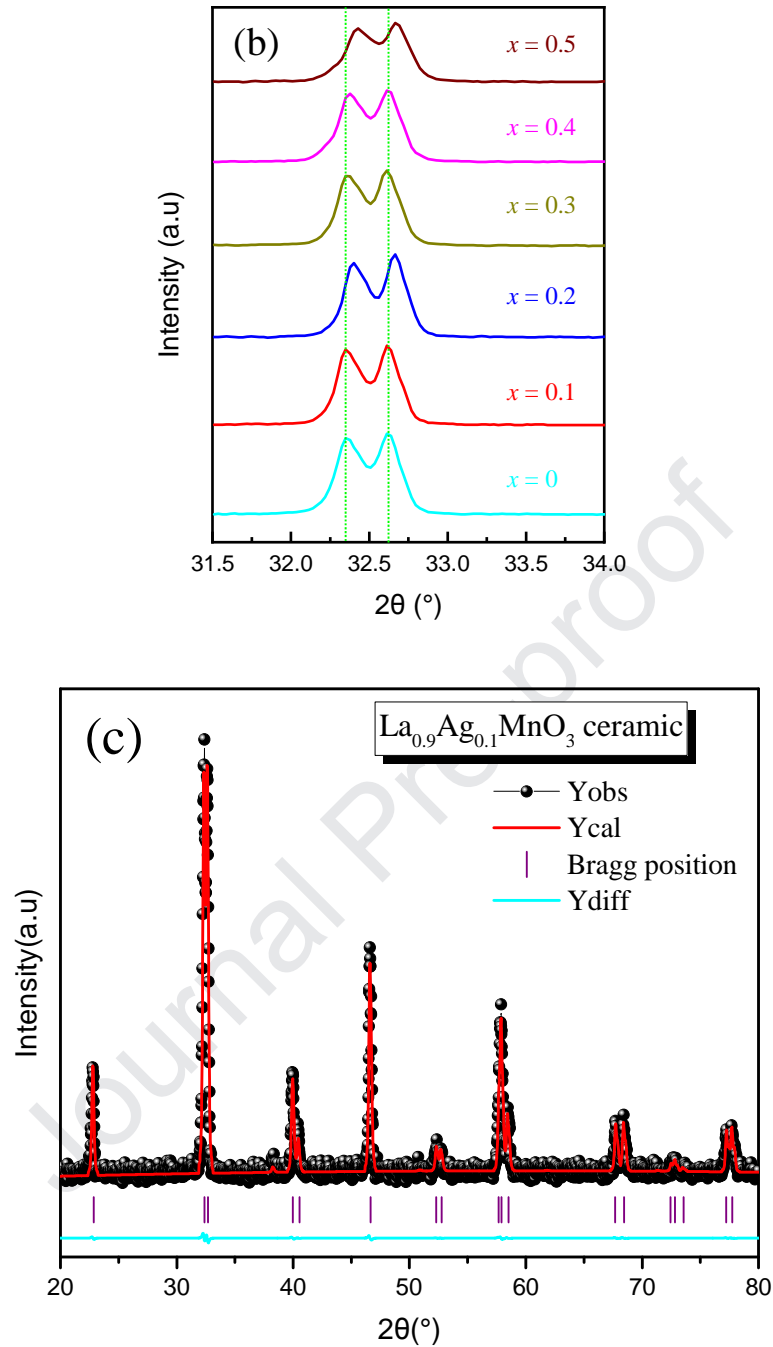


Fig.6. (a). X-ray diffraction patterns of the LAMO ($x = 0\sim 0.5$) polycrystalline ceramics. (b). Enlarged plot of main peaks in the 2θ range of $31.5\sim 34^\circ$. (c). Rietveld refined X-ray diffraction pattern of $\text{La}_{0.9}\text{Ag}_{0.1}\text{MnO}_3$ polycrystalline ceramics.

Table.2

The experiments and calculation for LAMO ($x = 0, 0.3, 0.5$) structure parameters lattice constant, cell volume, Mn–O bond length and angles and the R-factors of Rietveld

Structure parameters	LaMnO_3	$\text{La}_{0.7}\text{Ag}_{0.3}\text{MnO}_3$	$\text{La}_{0.5}\text{Ag}_{0.5}\text{MnO}_3$
	Exp/Cal	Exp/Cal	Exp/Cal

a (Å)	5.518/5.663	5.513/5.654	5.509/5.540
b (Å)	5.518/5.662	5.513/5.654	5.509/5.539
c (Å)	13.355/13.577	13.358/13.669	13.359/13.743
V (Å ³)	352.227/383.069	351.630/371.071	351.011/364.652
$\langle r_A \rangle$ (Å)	1.36	1.34	1.32
$d_{\text{Mn-O}}$ (Å)	1.967/2.089	1.965/1.985	1.964/1.984
$\theta_{\text{Mn-O-Mn}}$ (°)	162.184/155.500	162.187/154.496	162.188/159.833
R_p (%)	4.411	4.708	5.912
R_{wp} (%)	5.797	6.400	8.075
R_b (%)	5.389	5.416	5.291
χ	1.158	1.397	2.320

XRD was performed for LAMO ($x = 0, 0.1, 0.2, 0.3, 0.4$ and 0.5) polycrystalline ceramics. As seen in Fig 6 (a), unmarked peaks belong to perovskite structure LAMO, and marked peaks correspond to metal Ag with Mn_3O_4 phase. It was clear seen that the Mn_3O_4 (PDF#24-0734) phase occurs in the LAMO compound by Ag doping. At low Ag contents ($0 \leq x \leq 0.2$), the structure was mainly composed of perovskite structure phase and Mn_3O_4 phase. However, for $x \geq 0.3$, the metal Ag phase (PDF#04-0783) occurs in LAMO ceramics were composed of perovskite, Mn_3O_4 and metal Ag phase. These results suggested that the solubility limit of silver was around 0.3, which was in accordance with the different works of the literature had reported [13, 18, 29]. All polycrystalline ceramics exhibited rhombohedral perovskite phases with $R\bar{3}c$ space group, as shown in Fig 6 (b). The XRD Rietveld spectra of $\text{La}_{0.9}\text{Ag}_{0.1}\text{MnO}_3$ were studied, as shown in Fig 6 (c). Also, the results for Rietveld R-factors and structural parameters for LAMO ($x = 0, 0.3, 0.5$) ceramics are shown in Table 2. The LAMO structure (ICSD, 153552) to was used to fitting the XRD spectra

of $x \leq 0.2$. At high Ag contents ($0.3 \leq x \leq 0.5$), the LAMO structure (153552, from ICSD), metal Ag phase (PDF#04-0783) and Mn_3O_4 (PDF#24-0734) phase were used to fit the XRD result, respectively. Since La^{3+} ion (1.36 Å) was substituted by Ag^+ ion (1.28 Å), the average radius of A-site cation $\langle r_A \rangle$ decreased from 1.36 Å ($x = 0$) to 1.32 Å ($x = 0.5$). Meanwhile, the parameters a , b and Mn–O bond length were slightly shortened, whereas the parameter c and Mn–O bond angles showed minor expansion. This resulted in a smaller volume of the LAMO crystal structure due to doping of Ag. As the proportion of Ag doping enhanced, the changing of lattice parameters were consistent with previous studies [29]. Moreover, the average size of B-site cation was reduced with the increase of Mn^{4+} contents, since Mn^{4+} ion (0.53 Å) is smaller than Mn^{3+} ion (0.645 Å). The change in τ , is defined as:

$$\tau = \frac{r_A + r_O}{\sqrt{2}(r_B + r_O)} \quad (1)$$

Where r_i represents the radius of i ions, also play an importance role in Mn–O bond angles, leading the distortion of MnO_6 octahedron. Meanwhile, the parameters a , b and c based on DFT calculation of bulk structure LAMO ($x = 0, 0.3$ and 0.5) are also presented in Table 2. Comparing experiment with calculation results showed that a and b decreased from 5.518 to 5.510 and 5.663 to 5.540 Å for experiment and calculation results, respectively, as x varied from 0 to 0.5. The parameter of c showed a minor increase. As a result, the trend change of parameters calculations was in a good agreement with our experimental results.

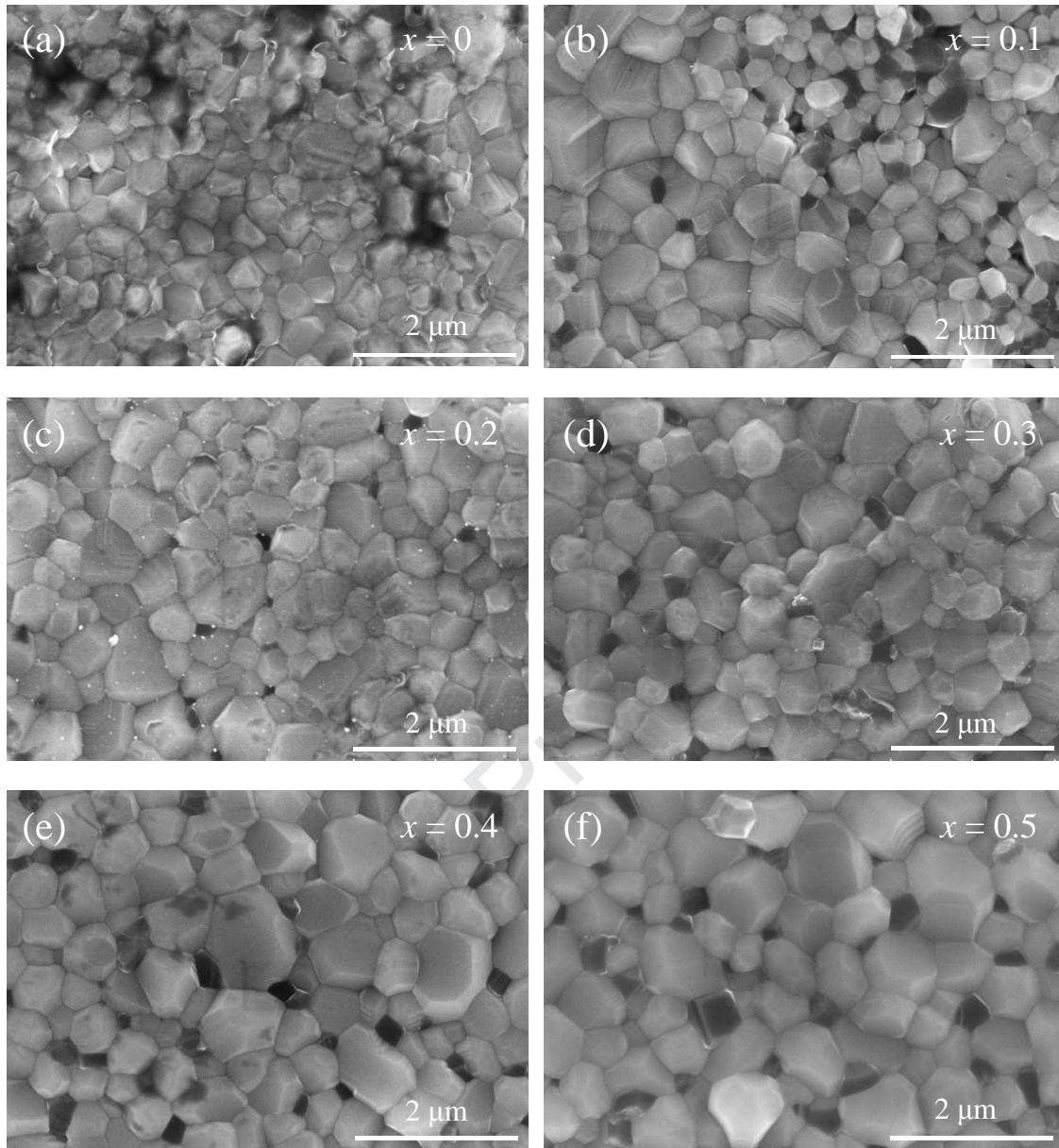


Fig.7. SEM images of $\text{La}_{1-x}\text{Ag}_x\text{MnO}_3$ samples. (a)~(f) represent $x = 0\sim 0.5$, respectively.

The surface morphologies of $\text{La}_{1-x}\text{Ag}_x\text{MnO}_3$ ($0 \leq x \leq 0.5$) samples at the same magnification of $2\ \mu\text{m}$ as shown in Fig 7(a)-(f). All samples displayed preferable compactness with few pores, and fine crystalline was obtained. The crystallinity was improved with Ag doping. The grain sizes were controlled by the doping addition, which the increased of grain sizes with Ag^+ doping increases were observed. In addition, the grain sizes have an effect on the number of grain boundaries, in turn

change the resistivity of $\text{La}_{1-x}\text{Ag}_x\text{MnO}_3$ samples.

3.3. Electrical transport and magnetic properties

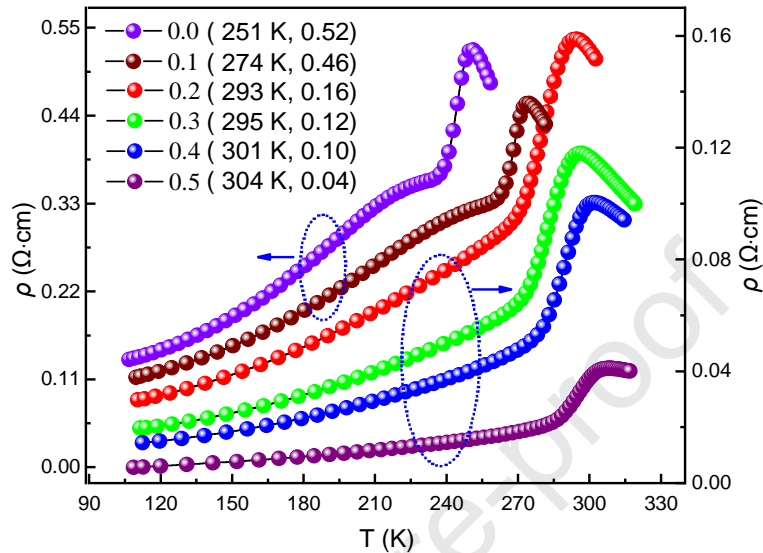


Fig.8. Plot of electrical resistivity as a function of temperature at 0 T for LAMO ($x = 0\sim 0.5$).

The resistivity as a function of temperature for LAMO ceramics in the temperature range of 100 to 320 K is shown in Fig 8. The peaks value of resistivity also listed in Fig 8. All ceramics exhibited ferromagnetic metallic property at low temperatures ($d\rho/dT > 0$) and paramagnetic insulator characteristics at high-temperatures ($d\rho/dT < 0$). The polaronic effect made the e_g and t_{2g} electrons to have the same spin alignment and displayed ferromagnetic metallic behavior at low-temperature. In contrast, for paramagnetic insulator behavior, the spin electrons were disordered between e_g and t_{2g} orbitals at high-temperature. Furthermore, as x was increased, the Mn e_g electrons transitioned from localized state to delocalized state, thereby leading to an increase in the conduction electron density of polycrystalline ceramics. It should be noted that the resistivity occurs sharp decrease at $x \geq 0.2$. The reasons might be caused by the

uniformly of grain sizes and grain boundaries. In Fig 7, we can see that the grain sizes were much uneven for $x = 0$ and 0.1. As x increasing ($0.2 \leq x \leq 0.5$), the grain sizes grow more evenly than low Ag contents, thereby might be result the reduction of the grain boundaries and grain boundaries scattering. The resistivity of LAMO decreased from 0.52 for $x = 0$ to 0.04 for $x = 0.5$. Meanwhile, the T_p increased from 251 K for $x = 0$ to 304 K (room temperature 300 K) for $x = 0.5$. Based on previous studies [30, 31], the JT and DE effect play an important role in insulators and metallic behavior, respectively. T_p improved with increasing x , and the JT and DE effect receded and enhanced, respectively. It was also in a good agreement with our calculation results.

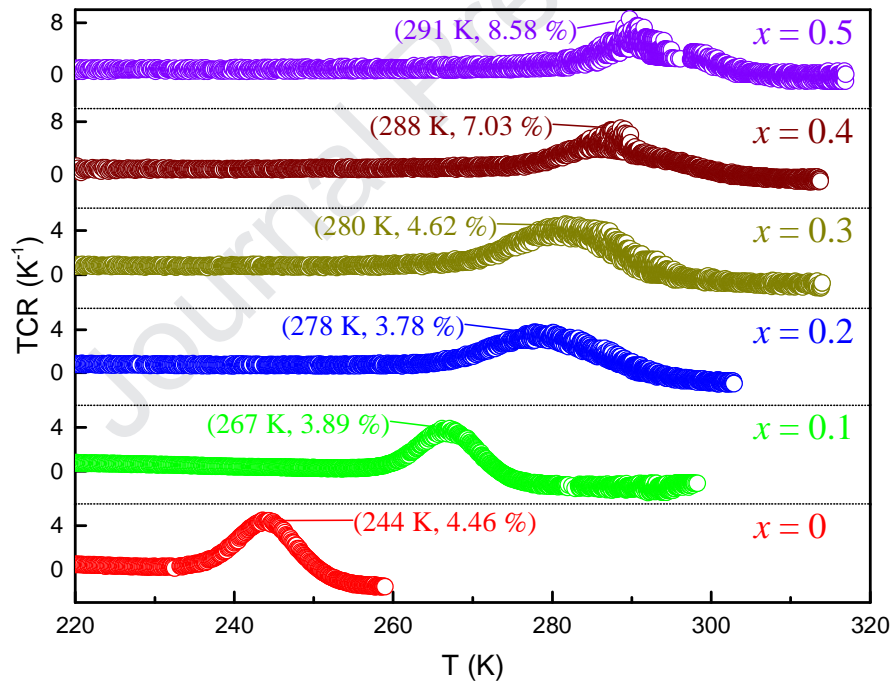


Fig. 9. The TCR (%) as a function of temperature for LAMO ($x = 0\sim 0.5$) polycrystalline ceramics.

The TCR (%) as a function of temperature for LAMO ($x = 0\sim 0.5$) ceramics is shown in Fig 9. The TCR is defined as follows:

$$TCR = \left(\frac{1}{\rho} \times \frac{d\rho}{dT} \right) \times 100\% \quad (2)$$

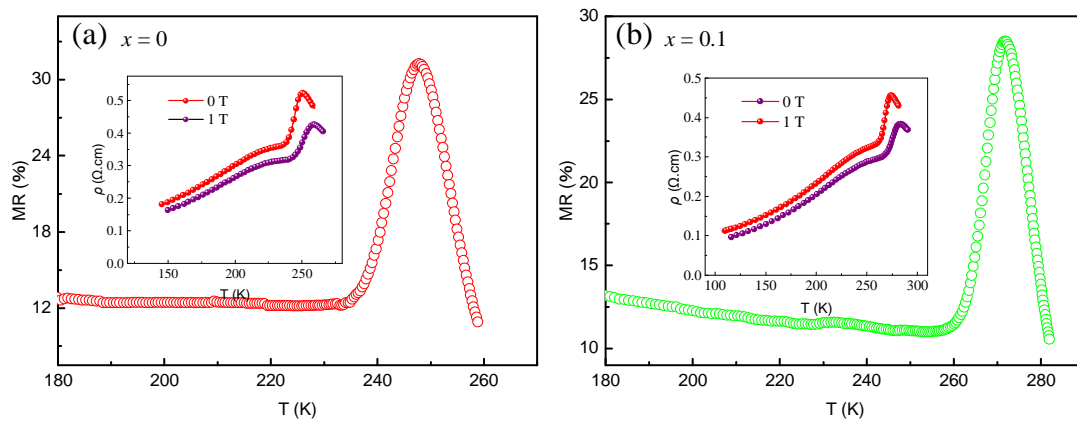
where, ρ and T are resistivity and temperature, respectively. With increasing of x , the TCR peak temperatures (T_k) increased from 244 K for $x = 0$ to 291 K for $x = 0.5$. The values of TCR decreased first and then increased, from 4.46 % for $x = 0$ to 8.58 % for $x = 0.5$. At $x = 0.5$, the TCR reached a maximum value of 8.58% and T_k reached room temperature (291 K). The peak TCR value depends on many factors, including sintering temperature, preparation method, grain sizes, the tolerance factor τ and the resistivities of the samples. At low Ag contents ($0 \leq x \leq 0.2$), the reduction of TCR values might be caused by the replacement of La ion by Ag results in a decrease of the tolerance factor τ . As Ag content increased to a certain extent ($x > 0.2$), the influence of resistivity and grain sizes play a dominant role in the peak TCR values. The samples resistivities significant reductions and grain sizes were improved, which led to the peak TCR values increased. In addition, the Ag occurs in the form of the second phase at grain boundaries and interfaces open a new channel for the electron transport, which leading to decreases the ρ of the samples and TCR increased. Meanwhile, based on previous reports [32], increasing the conductivity along with an enhanced DE effect should gradually increase TCR . These data suggested that high TCR value of this report polycrystalline ceramics could potentially impact their applications in uncooled bolometers or infrared detectors at room-temperature.

The MR is defined as:

$$MR(\%) = \left(\frac{\rho_0 - \rho_H}{\rho_0} \right) \times 100\% \quad (3)$$

where, ρ_0 and ρ_H are resistivity at 0 and 1 T magnetic field, respectively. The MR

versus temperature for LAMO ($x = 0\sim 0.5$) is shown in Fig 10. A magnetic field of 1 T resulted in the increased ordering of electron spins of Mn^{3+} and Mn^{4+} , and it was easier for electrons to transition between Mn^{3+} and Mn^{4+} ions as compared to the 0 T case. Thus, the resistivity at 0 T was higher than 1 T. The *MR* curve displayed a similar variation with increasing temperature, which it initially increased and then decreased. T_m increased from 248 K ($x = 0$) to 298 K ($x = 0.5$), which was obtained at room temperature. The values of *MR* decreased from 31.3% ($x = 0$) to 21.6% ($x = 0.5$) at room temperature. Two types of *MR* have been confirmed in perovskite manganites oxides, intrinsic and extrinsic *MR*, which induced by DE effect and tunneling effects between the grain boundaries (GBs), respectively. It was noted that the spin-polarized tunneling phenomenon for GBs play a key role in the *MR* properties, because of the values of *MR* were decreases gradually with GBs increasing. Meanwhile, based on previous research [1, 33], the spin-polarized tunneling phenomenon could have an important influence on *MR*, and the enhanced spin disorder with increasing x led to lower *MR*. Meanwhile, the diamagnetic feature of Ag was also one of factor for the lowering of *MR*.



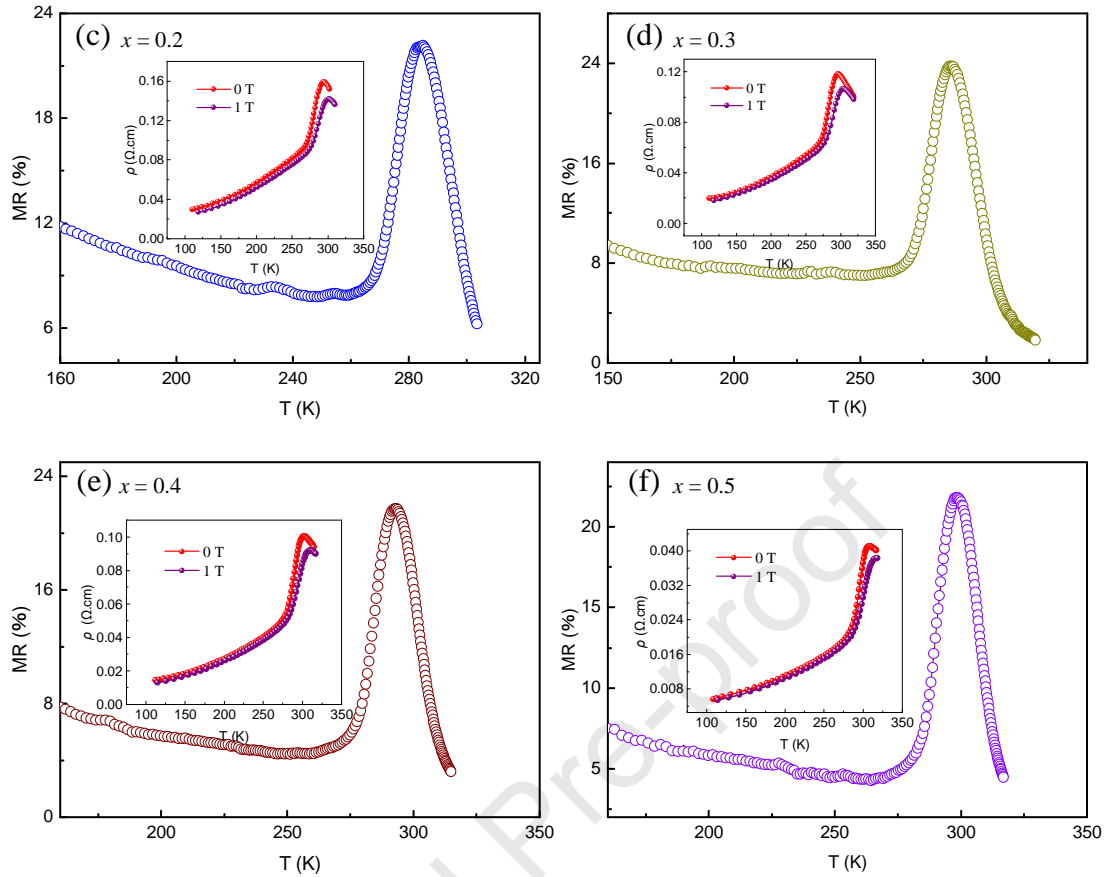


Fig. 10. The MR (%) as a function of temperature for LAMO ($x = 0 \sim 0.5$) samples at 1 T magnetic field. (a~f) represent the doping $x = 0 \sim 0.5$, respectively. The inset graph is ρ - T curves under different magnetic field (0 T, 1 T).

A summary of the T_p , T_k , T_m , TCR and MR with the different of x level is shown in Table 3. Results indicated that the T_p , T_k , T_m , TCR and MR could be controlled by the doping x level. With the increasing x , the T_p , T_k , T_m and TCR were augmented but MR declined. At $x = 0.5$, the high TCR (8.58 %) and MR (21.6 %) were obtained at room temperature, which means that the LAMO ceramics could be used for photoelectric or magnetic devices at room temperature.

Table 3.

The values of T_p , T_k , T_m , TCR and MR for LAMO ($x = 0 \sim 0.5$) polycrystalline ceramics.

x (mol%)	0.0	0.1	0.2	0.3	0.4	0.5
T_p (K)	251	274	293	295	301	304

TCR (%)	4.46	3.89	3.78	4.62	7.03	8.58
T_k (K)	244	267	278	280	288	291
MR (%)	31.3	28.5	22.1	23.8	21.7	21.6
T_m (K)	248	272	284	286	292	298

3.4 Analysis of XPS results

The XPS spectra of Mn 2p and Ag 3d levels shown in Fig 11 indicate that the doping of Ag was successful in the LMO ceramics. For Fig 11 (a), as $x = 0$, the binding energies (BE) of Mn 2p_{1/2} and Mn 2p_{3/2} orbital were 653.38 eV and 641.73 eV, respectively. For $x = 0.5$, the BE of Mn 2p_{1/2} and Mn 2p_{3/2} levels were 653.13 eV and 641.63 eV, respectively, as shown in Fig 11 (b). Compared to $x = 0$, the BE of Mn 2p_{1/2} and Mn 2p_{3/2} orbitals for $x = 0.5$ shifted to lower energy. In addition, as shown in Fig 11 (a) and (b), the value of BE Mn 2p_{3/2} level was between the Mn₂O₃ (641.4 eV) and MnO₂ (641.8 eV), which was indicative of Mn ions existing as Mn⁴⁺ and Mn³⁺. The fitting curve for different of x level doping was also measured. The concentration of Mn⁴⁺ in (Mn³⁺ + Mn⁴⁺) was estimated to 20.54% and 33.29% for $x = 0$ and 0.5, respectively. Thus, ratio of Mn⁴⁺/Mn³⁺ was characterized from 1 : 4 for $x = 0$ to 1 : 2 for $x = 0.5$, which indicated that the concentration of Mn⁴⁺ increased and DE effect enhanced with the increasing of x . Furthermore, the volatilization of Ag might leading to the formation of the vacancies on La and O sites, these also play an important role in the valence state of Mn. Meanwhile, the XPS spectra for $x = 0$ and 0.5 polycrystalline ceramics was determined, the different elements orbital were labeled in Fig 11 (c). The replacement of La ion by Ag results in a decrease of the La 3d_{3/2} and 3d_{5/2} level for $x = 0.5$, And the Ag⁰ and Ag⁺ level occurs for $x = 0.5$ compared to $x = 0$,

which was good agreement with XRD results. Otherwise, in order to obtain the existence form of Ag for $x = 0.5$, the Ag 3d level spectrum was measured for $x = 0.5$ as seen in Fig 11 (d). The BE of Ag 3d_{3/2} and Ag 3d_{5/2} orbitals were 374 eV and 368 eV, respectively. Based on previous studies [34-36], the BE of Ag 3d_{5/2} was between the value for Ag⁰ (368.7 eV) and Ag⁺ (367.6 eV), which indicated that the metal Ag and Ag⁺ coexisted for $x = 0.5$. Meanwhile, the difference of binding energy between Ag 3d_{3/2} and Ag 3d_{5/2} was 6.0 eV, which indicated that the metal Ag existed in $x = 0.5$ [37]. This was also in agreement with XRD patterns.

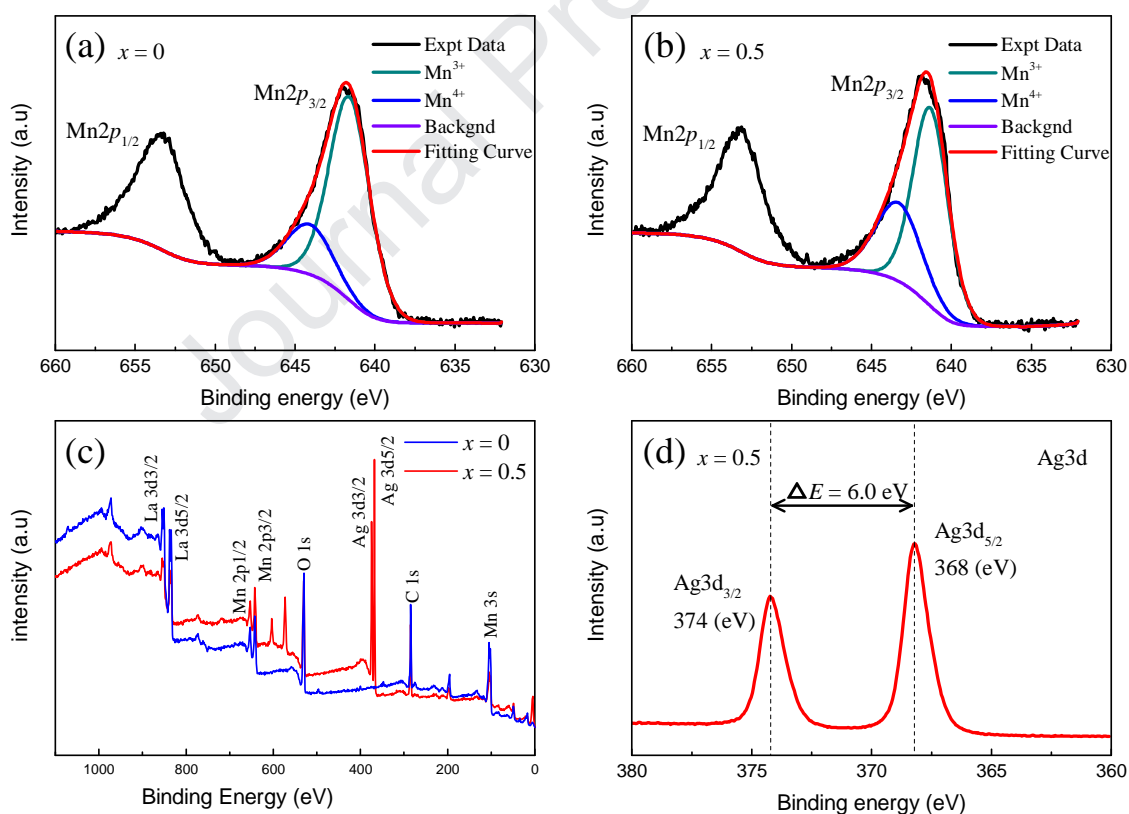


Fig. 11. (a), (b) Mn 2p levels spectra and fitting curve for LAMO ($x = 0$ and 0.5), respectively. (c) XPS spectra for LAMO ($x = 0$ and 0.5) and (d) Ag 3d level spectra for LAMO ($x = 0.5$).

4. Conclusions

In summary, the electronic structures of LAMO ($x = 0, 0.3, 0.5$) polycrystalline ceramics with rhombohedra structure were calculated by CASTEP with DFT by first principles calculations method, using the GGA + U within PBE approach. The band gap and DOS were also studied for LAMO ceramics. For $x = 0, 0.3$ and 0.5 , the E_i and E_d were 1.29, 0.37, 0.06 eV and 1.51, 0.79, 0.23 eV, respectively. The PDOS indicated that the energy difference of $E(e_{g\uparrow}^2) - E(e_{g\uparrow}^1)$ decreased and Hund coupling between Mn e_g and t_{2g} increased with increasing x . Correspondingly, the JT and DE effect decreased and enhanced, respectively. LAMO ($x = 0\sim 0.5$) polycrystalline ceramics were prepared by the sol-gel method in order to verify the first principles calculations results. The structure, electrical and magnetic properties of LAMO samples were studied in details. XRD results showed that all polycrystalline ceramics were rhombohedra structure with $\bar{R}3c$ space group, and a single phase to multiphase transition was observed. For $x < 0.3$, the ceramics were only composed of perovskite phase. For $x \geq 0.3$, multiphase characteristics were obtained with perovskite phase, metal Ag and Mn_3O_4 . The experimental and calculations results on the crystal structure suggested that the doping of Ag led to a volume reduction of LAMO ceramics, wherein the Mn-O bond length was found to decrease and angles were expanded. In addition, $\rho-T$ curves were studied as a function of x . Results showed that the T_p improved and DE effect enhanced, which was in good agreement with the calculation results. Furthermore, as x increased, T_p , T_k and T_m increased, the TCR decreased first and then increased, and the MR declined gradually. At $x = 0.5$, T_p , T_k

and T_m were 304, 291 and 298 K near room temperature. Furthermore, the Mn^{4+}/Mn^{3+} amount was studied by XPS, where an enhanced concentration of Mn^{4+} was obtained with increasing of x . The value of Mn^{4+}/Mn^{3+} was 1 : 4 for $x = 0$ and 1 : 2 for $x = 0.5$. This indicated that LAMO ceramics had the strongest DE effect at doping level $x = 0.5$, where Mn^{4+} converted into Mn^{3+} (Mn^{4+}/Mn^{3+} ratio at 1:2). These results suggest promising applications of LAMO polycrystalline ceramics in photoelectric or magnetic devices at room temperature.

Acknowledgements

This work was financially supported by the National Natural Science Foundation of China (Grant no. 11674135), the Analysis and Testing Foundation of Kunming University of Science and Technology (Grant no. 2018M20172130001), and the Innovation Training Program for College Students, (Grant no. 20180179).

References

- [1] S. Zhao, X. Yue, X. Liu, Tuning room temperature T_p and MR of $La_{1-y}(Ca_{y-x}Sr_x)MnO_3$ polycrystalline ceramics by Sr doping, *Ceramics International*, 43 (2017) 4594-4598.
- [2] T. Sun, S. Zhao, F. Ji, X. Liu, Enhanced room-temperature MR and TCR in polycrystalline $La_{0.67}(Ca_{0.33-x}Sr_x)MnO_3$ ceramics by oxygen assisted sintering, *Ceramics International*, 44 (2018) 2400-2406.
- [3] D. Rybicki, M. Sikora, J. Przewoznik, C. Kapusta, J.F. Mitchell, Interplay of local structure, charge, and spin in bilayered manganese perovskites, *Physical Review B*, 97 (2018).
- [4] Y. G. Tang, G. Y. Wang, G. Q. Yan, Q. X. Song, M. Y. Zhang, Z. S. Peng, Temperature stability of magnetoresistance (MR) and MR enhancement in $La_{1-x}(Sr_{1-y}Ag_y)_xMnO_3$ system, *Rare Metals*, 32 (2013) 81-86.
- [5] F. Jin, H. Zhang, Q. Chen, Improved Curie temperature and temperature coefficient of

- resistance (TCR) in $\text{La}_{0.7}\text{Ca}_{0.3-x}\text{Sr}_x\text{MnO}_3:\text{Ag}_{0.2}$ composites, *Journal of Alloys and Compounds*, 747 (2018) 1027-1032.
- [6] S. Keshri, S. Biswas, P. Wiśniewski, Studies on characteristic properties of superparamagnetic $\text{La}_{0.67}\text{Sr}_{0.33-x}\text{K}_x\text{MnO}_3$ nanoparticles, *Journal of Alloys and Compounds*, 656 (2016) 245-252.
- [7] J.B. Goodenough, Electronic structure of CMR manganites, *J. Appl. Phys.*, 81 (1997) 5330-5335.
- [8] F. K. B. Sajid Ur Rehman, Bakhtiar Ul Haq, Salem AlFaify, Waheed S. Khan, Chuanbo Li, Exploring novel phase of tin sulfide for photon_energy harvesting materials, *Solar Energy*, 169 (2018) 648-657.
- [9] B. U. H. Faheem K. Butt, Sajid ur Rehman. Ahmed, Chuanbao Cao, S. AlFaifi, Investigation of thermoelectric properties of novel cubic phase SnSe: A promising material for thermoelectric applications, *Journal of Alloys and Compounds*, 715 (2017) 438-444.
- [10] A. R. Bushra Tehseen, Muniba Rahmat, Haq Nawaz Bhatti, Aiguo Wu, Faheem K. Butt, Gul Naz, Waheed S. Khan, Sadia Z. Bajwaa, Solution growth of 3D MnO_2 mesh comprising 1D nanofibres as a novel sensor for selective and sensitive detection of biomolecules, *Biosensors and Bioelectronics*, 117 (2018) 852-859.
- [11] A. Granovskii, B. Y. Sukhorukov, P. A. Telegin, V. Giant magnetorefractive effect in $\text{La}_{0.7}\text{Ca}_{0.3}\text{MnO}_3$ films, *J. Exp. Theor. Phys.*, 112 (2011) 77-86.
- [12] A.G. Gamzatov, A.M. Aliev, K.S. Khizriev, I.K. Kamilov, A.S. Mankevich, Critical behavior of $\text{La}_{0.87}\text{K}_{0.13}\text{MnO}_3$ manganite, *Journal of Alloys and Compounds*, 509 (2011) 8295-8298.
- [13] K.M.G. T.Tang, Q.Q.Cao, Magnetometric properties of Ag substituted perovskite-type manganites, *Journal of Magnetism and Magnetic Materials*, 222 (2000) 110-114.
- [14] K. H. K. J. H. Jung, D. J. Eom and T. W. Noh, Determination of electronic band structures of CaMnO_3 and LaMnO_3 using optical-conductivity analyses, *Physical Review B*, 55 (1997) 23.
- [15] A. Millis, J. P. Littlewood, B. Double Exchange Alone Does Not Explain the Resistivity of $\text{La}_{1-x}\text{Sr}_x\text{MnO}_3$, *Physical review letters*, 74 (1995).
- [16] J. Jiang, S. Zhao, T. Sun, Q. Chen, X. Liu, Influence of Ag doping on electrical and magnetic properties of $\text{La}_{0.625}(\text{Ca}_{0.315}\text{Sr}_{0.06})\text{MnO}_3$ ceramics, *Ceramics International*, (2017).
- [17] J. Jiang, Q. M. Chen, X. Liu, First-principles study on the electronic structure and optical properties of $\text{La}_{0.75}\text{Sr}_{0.25}\text{MnO}_{3-\sigma}$ materials with oxygen vacancies defects, *Current Applied Physics*,

18 (2018) 200-208.

[18] L. S. Ye., H. W. Song., M. J. Dai., Y. K. Wang., G. S. Wang., L. C. Zhang., J. J. Du., P. Y. Sun., F. J. Effect of Ag substitution on the transport property and magnetoresistance of LaMnO₃, Journal of Magnetism and Magnetic Materials, 248 (2002) 26-33.

[19] J.P. Perdew, K. Burke, M. Ernzerhof, Generalized Gradient Approximation Made Simple, Physical review letters, 77 (1996).

[20] M. Pavone, A.B. Muñoz-García, A.M. Ritzmann, E.A. Carter, First-Principles Study of Lanthanum Strontium Manganite: Insights into Electronic Structure and Oxygen Vacancy Formation, The Journal of Physical Chemistry C, 118 (2014) 13346-13356.

[21] L.C. Moreno, J.S. Valencia, D.A. Landínez Téllez, J. Arbey Rodríguez M, M.L. Martínez, J. Roa-Rojas, F. Fajardo, Preparation and structural study of LaMnO₃ magnetic material, Journal of Magnetism and Magnetic Materials, 320 (2008) e19-e21.

[22] C. Franchini, R. Kovacik, M. Marsman, S.S. Murthy, J. He, C. Ederer, G. Kresse, Maximally localized Wannier functions in LaMnO₃ within PBE + U, hybrid functionals and partially self-consistent GW: an efficient route to construct ab initio tight-binding parameters for e_g perovskites, Journal of physics. Condensed matter : an Institute of Physics journal, 24 (2012) 235602.

[23] M.H. Seo, H.W. Park, D.U. Lee, M.G. Park, Z. Chen, Design of Highly Active Perovskite Oxides for Oxygen Evolution Reaction by Combining Experimental and ab Initio Studies, ACS Catalysis, 5 (2015) 4337-4344.

[24] A.L. Gavin, G.W. Watson, Modelling the electronic structure of orthorhombic LaMnO₃, Solid State Ionics, 299 (2017) 13-17.

[25] T. Arima, Y. Tokura, J.B. Torrance, Variation of optical gaps in perovskite-type 3d transition-metal oxides, Physical Review B, 48 (1993) 17006-17009.

[26] T. Saitoh, A.E. Bocquet, T. Mizokawa, H. Namatame, A. Fujimori, M. Abbate, Y. Takeda, M. Takano, Electronic structure of La_{1-x}Sr_xMnO₃ studied by photoemission and X-ray absorption spectroscopy, Physical Review B, 51 (1995) 13942-13951.

[27] Y. Zhou, Z. Lü, P. Guo, Y. Tian, X. Huang, W. Su, First-principles study on the catalytic role of Ag in the oxygen adsorption of LaMnO₃(001) surface, Applied Surface Science, 258 (2012) 2602-2606.

- [28] J. Jung, H. K. Kim, H. D. Eom, J. T. Noh, W. Determiation of electronic band structures of CaMnO_3 and LaMnO_3 using optical-conductivity analyses, *Phys Rev B*, 55 (1997).
- [29] M.B. Bellakki, C. Shivakumara, N.Y. Vasanthacharya, A.S. Prakash, Rapid synthesis of room temperature ferromagnetic Ag-doped LaMnO_3 perovskite phases by the solution combustion method, *Materials Research Bulletin*, 45 (2010) 1685-1691.
- [30] D. Cao, Y. Zhang, W. Dong, J. Yang, W. Bai, Y. Chen, G. Wang, X. Dong, X. Tang, Structure, magnetic and transport properties of $\text{La}_{0.7}\text{Ca}_{0.3-x}\text{Sr}_x\text{MnO}_3$ thin films by sol-gel method, *Ceramics International*, 41 (2015) S381-S386.
- [31] B.M.n. J. Fontcuberta, A. Seffar, S. Piñol, J. L. García-Muñoz, and X. Obradors, Colossal Magnetoresistance of Ferromagnetic Manganites_ Structural Tuning and Mechanisms, *Physical review letters*, 76 (1996).
- [32] X. J. Y. Shuang Zhao, Xiang Liu, Influence of Sr doping on structural, electrical and magnetic properties of $\text{La}_{0.7}\text{Ca}_{0.3}\text{MnO}_3$ nanoparticles., *Ceramics International*, 43 (2017) 13240-13246.
- [33] C. Xiong, H. Hu, Y. Xiong, Electrical properties and enhanced room temperature magnetoresistance in $(\text{La}_{0.7}\text{Ca}_{0.2}\text{Sr}_{0.1}\text{MnO}_3)_{1-x}\text{Pd}_x$ composites, *Journal of Alloys & Compounds*, 479 (2009) 357-362.
- [34] S. A. Park, H. Lim, Y. T. Kim, Enhanced Oxygen Reduction Reaction Activity Due to Electronic Effects between Ag and Mn_3O_4 in Alkaline Media, *ACS Catalysis*, 5 (2015) 3995-4002.
- [35] Y. Xue, H. Miao, S. Sun, Q. Wang, S. Li, Z. Liu, $\text{La}_{1-x}\text{Ag}_x\text{MnO}_3$ electrocatalyst with high catalytic activity for oxygen reduction reaction in aluminium air batteries, *RSC Adv*, 7 (2017) 5214-5221.
- [36] J. Ohyama, Y. Okata, N. Watabe, M. Katagiri, Oxygen reduction reaction over silver particles with various morphologies and surface chemical states, *Journal of Power Sources*, 245 (2014) 998-1004.
- [37] W. Alshammari, D. S. Patil, S. A. Pawar, J. C. Shin, Silver nanowires-copper sulfide core/shell nanostructure for electrochemical supercapacitors, *Materials Today Chemistry*, 5 (2017) 72-80.

1. Electromagnetic properties of LAMO were explored by abinitio/experimental methods.
2. *TCR* and *MR* reached $8.58\% \text{ K}^{-1}$ and 21.6% as T_k and T_m at 291 and 298 K respectively.
3. DE and JT were used to explain improvement of electromagnetic properties for LAMO.
4. The results indicated promising applications of LAMO in room temperature devices.